SURFACE DISCHARGE ARC PROPAGATION AND DAMAGE ON SPACECRAFT DIELECTRICS

K G Balmain

University of Toronto
Department of Electrical Engineering, Toronto, Canada

ABSTRACT

The propagation of a surface discharge arc or flashover on dielectrics such as Mylar, Teflon and Kapton is the mechanism by which 10-30 keV deposited electronic charge is mobilized to produce damaging arc current densities. A propagation mechanism is discussed, in which the progress of the surface arc is controlled by the rate of removal of excess charge along filamentary tunnels filled with an overdense plasma of ionized discharge debris. Supporting evidence is drawn from area-scaling measurements of discharge electrical properties, and from microscope photographs of permanent damage in the form of sub-micron-diameter subsurface tunnels and surface grooves.

Keywords: Dielectric Arc Propagation, Dielectric Arc Damage, Dielectric Flashover, Spacecraft Discharge, Spacecraft Charging.

1. INTRODUCTION

Spacecraft charging by incident energetic electrons and consequent arc discharging are now reasonably well-established phenomena (Refs. 1-4) which apparently have caused synchronous-orbit satellites to exhibit various types of operational anomalies. To date, retrieval of synchronous-orbit spacecraft has not been possible, so the relevant experimental research results have come largely from ground-based laboratories. These measurements have shown that the incident electrons become embedded a few microns beneath the surface of any exposed dielectric materials on the spacecraft outer surface. When a sufficient charge has accumulated, breakdown occurs and propagates swiftly over the charged region as a surface "flashover". This discharge is accompanied by electron ejection with corresponding replacement current flow into the interior of the spacecraft, current which very probably can reach peak values of hundreds of amperes for dielectric sheet areas of the order of one square meter.

Laboratory measurements of the replacement current pulses resulting from these discharges have shown that the peak current and as well the released charge, pulse duration and energy dissipated in a load resistor all follow well-defined scaling laws as the specimen area is varied (Refs. 5,6,7), and furthermore these scaling laws are similar for Kapton, Teflon and Mylar (Ref. 8). For example, the peak discharge current has been found to scale in proportion to the area raised to the power 0.5 approximately, or in other words 0.5 is the slope of the corresponding log-log graph of peak current versus area. Similarly the log-log graphs of released charge, pulse duration and energy dissipated in a load resistor respectively exhibit slopes of 1.0, 0.5 and 1.5 approximately.

Discharge surface damage has also been identified on Kapton, Mylar and Teflon (Refs. 6,7,8,9). This damage takes the form of surface grooves, subsurface tunnels, "punchthrough" holes, and "blowout" holes. The appearance of this damage and the lightning-like appearance of the light emitted from a flashover arc suggest that the discharge arc propagates across the dielectric surface, and the velocity of propagation has been estimated (Refs. 6,8) by dividing the specimen radius by the pulse duration, giving approximately 3×10^5 m/s. The discharge propagation mechanism has been postulated to be due to "electron-hopping" (Ref. 10), to be controlled by the inductance and capacitance of a conducting channel (Ref. 11), and to involve wave propagation along a plasma channel (Ref. 8).

This study contains a further examination of the plasma channel propagation concept, and includes additional evidence in the form of photographs of damage patterns all having the forms of surface or subsurface channels.

2. THE PLASMA CHANNEL

That a discharge in a solid dielectric could develop in the form of a plasma channel was argued in considerable detail by Budenstein (Ref. 12), but the velocity of propagation of the arc is yet to be explained. Whatever the mechanism for propagation, the existence of a finite velocity is probably what determines the 0.5 slope of the peak current versus area curve. This can be seen by imagining the discharge to be in the form of a wave expanding from an ignition point, the resultant replacement current being proportional to the length of the wavefront. Clearly the maximum length of the wavefront is proportional to the linear dimensions of the specimen or in other words proportional to the square root of the area as observed. It would appear that an arc discharge propagating along straight, branching paths produces the same area-scaling effect.

To devise a model for discharge propagation, one must first take note of the experimental configuration shown in Figure 1. The charged area on

Proceedings of an ESA Symposium on Spacecraft Materials, held at ESTEC, 2-5 October 1979 – ESA SP-145 (December 1979).

the dielectric sheet is defined by a tight-fitting metal mask which has a bevelled edge to reduce emitted-electron interception. The incident electrons become embedded in a diffuse layer 5 to 8 μm below the surface, with resultant high electric field being set up both above and below the charge layer (Refs. 13,14) and adjacent to the mask edge. Breakdown can be initiated at any high-field point, resulting in a punchthrough arc to the substrate (bulk breakdown), a blowoff arc to the surface, or a flashover arc consisting of a propagating subsurface discharge terminating in either a blowout hole or a punchthrough hole.

Such a propagating subsurface discharge is sketched in Figure 2. It is postulated that enough energy is released in the breakdown process to maintain a plasma channel of ionized debris connecting the point of discharge to the outside vacuum region. Because breakdown requires a high local field, it is further postulated that the excess charge must be removed via the plasma channel before each step in the breakdown process can proceed. The extent of the high field region ahead of the point of discharge should be about the same as the distance travelled by the excess charge along the channel, in a given time interval, so that the velocity of propagation of the discharge should be approximately equal to the velocity of propagation of the excess charge along the plasma channel.

In earlier work (Ref. 8) it was noted that an electromagnetic wave on a highly conducting channel over a highly conducting ground plane would propagate at the velocity of light in the dielectric medium, but the observed velocity appears to be almost three orders of magnitude lower. It was postulated in the earlier work that the required wave slowing could be produced by the added inductance per unit length provided by an overdense plasma channel, the inductance per unit length contributed by the plasma being

$$L_p = \frac{1}{\pi a^2 \epsilon_o \omega_p^2} = \frac{m}{\pi a^2 N e^2} \tag{1}$$

for a plasma relative permittivity given by

$$\epsilon_p = 1 - \frac{\omega_p^2}{\omega^2} \tag{2}$$

$$\simeq -\frac{\omega_p^2}{\omega^2} \quad \text{in the overdense case} \tag{3}$$

in which ω is the wave frequency (radians/s) for an $\exp(j\omega t)$ time variation, $\omega_p = (Ne^2/m\epsilon_o)^{\frac{1}{2}}$ is the plasma frequency, N is the electron density (m^{-3}), e is the electron charge magnitude (coul.), m is the electron mass (kg.), a is the channel radius and ϵ_o is the permittivity of a vacuum. It was indicated in the earlier work that the other contributions to the inductance per unit length were negligible, and therefore that the propagation velocity is

$$v_p = \frac{1}{(L_p C)^{\frac{1}{2}}} \tag{4}$$

where C is the capacitance per unit length given by $C = 2\pi\epsilon/[\cosh^{-1}h/a]$, h being the height of the plasma channel over the ground plane and $\epsilon=\epsilon_o\epsilon_d$ being the dielectric permittivity. Taking the logarithm approximation for $\cosh^{-1}$ and setting $\omega_p=2\pi f_p$ gives

$$v_p \simeq \frac{2\pi a\sqrt{\ln(2h/a)}}{\sqrt{\epsilon_d}} f_p \tag{5}$$

$$\simeq 2\sqrt{2}\ \pi\ a\ f_p \tag{6}$$

$$\simeq 9\ a\ f_p \tag{7}$$

in which the values $\epsilon_d = 3$, $h = 6\times10^{-5}$ m and $a = 3\times10^{-7}$ m have been used. Thus a velocity of 3×10^5 m/s would be produced by a plasma frequency f_p of 100 GHz, corresponding to an electron density of approximately 10^{20} m^{-3}.

The above calculation involves both elementary transmission-line theory and the inclusion of the ground plane. Conceivably these two constraints might in some way limit the accuracy of the calculated results, so there is reason to consider propagation along a cylindrical plasma channel of radius "a" and with relative permittivity $\epsilon_p = 1-\omega_p^2/\omega^2 = -\omega_p^2/\omega^2$ inside an infinite dielectric of relative permittivity ϵ_d. The azimuthally symmetric Bessel-function TM solution is appropriate (Ref. 15) and its longitudinal electric field is

$$E_z = A\, J_o(\gamma_p\rho)\, e^{-j\beta z} \qquad \rho<a \tag{8}$$

$$E_z = C\, K_o(\gamma_d\rho)\, e^{-j\beta z} \qquad \rho>a \tag{9}$$

where $\gamma_p^2 + \beta^2 = k_p^2$, $k_p = \omega\sqrt{\mu_o\epsilon_o\epsilon_p}$ (10)

$$-\gamma_d^2 + \beta^2 = k_d^2, \quad k_d = \omega\sqrt{\mu_o\epsilon_o\epsilon_d} \tag{11}$$

The procedure of matching all tangential fields at $\rho=a$ gives $\gamma_p a \frac{J_o(\gamma_p a)}{J_1(\gamma_p a)} = -\frac{\epsilon_p}{\epsilon_d}\gamma_d a \frac{K_o(\gamma_d a)}{K_1(\gamma_d a)}$ (12)

On the assumption that a is small, the small-argument and overdense-plasma approximations give for equation (12)

$$-\frac{2\omega^2\epsilon_d}{\omega_p^2} = (\gamma_d a)^2 \ln(\gamma_d a) \tag{13}$$

Also, (11) can be written as

$$\frac{\omega^2}{v_p^2} = \frac{\omega^2}{c^2}\epsilon_d + \gamma_d^2 \tag{14}$$

To a first order of approximation, the slowly varying $-\ln(\gamma_d a)$ can be set equal to a constant M lying in the range 4.6 to 9.2 for values of $\gamma_d a$ in the range 10^{-2} to 10^{-4}. Thus (13) becomes

$$\frac{2}{M}\frac{\omega^2}{\omega_p^2}\epsilon_d = \gamma_d^2 a^2 \tag{15}$$

Eliminating γ_d from (15) and (14) gives

$$\frac{1}{v_p^2} = \frac{\epsilon_d}{c^2} + \frac{2\epsilon_d}{M\omega_p^2 a^2} \tag{16}$$

The term involving the velocity of light c is negligible, so that the plasma channel propagation velocity v_p is given by

$$v_p = \left(\frac{M}{2\epsilon_d}\right)^{\frac{1}{2}} a\, 2\pi\, f_p \qquad (17)$$

$$\text{or for } M \approx 8,\ v_p \approx 7\, a\, f_p \qquad (18)$$

which is almost identical to equation (7). Setting the logarithm in (13) equal to a constant implies the disregard of a small amount of wave dispersion and therefore the disregard of a small amount of resultant pulse distortion as the wave propagates. It is therefore clear that the use of transmission-line theory and the consideration of a nearby ground plane do not unduly restrict the original simplified analysis (Ref. 8), so that comparison with other theories (eg. Ref. 16) may be facilitated.

3. SURFACE DAMAGE

In the manner indicated in Figure 1, specimens of Kapton H, FEP Teflon and Mylar were exposed to a 20 kV electron beam of ±15% worst-case nonuniformity over the aperture and current density of 80 nA/cm^2. This current density is at least an order of magnitude higher than at synchronous orbit and was chosen in part to produce a high enough discharge repetition rate for convenient pulse averaging. Experiments suggested no significant change in individual discharge pulse properties from current densities of 10 μA/cm^2 down to 75 nA/cm^2, but more recent results (Ref. 17) suggest possible current density dependence of released charge and peak current below 8 nA/cm^2.

A typical arc discharge is shown in Figure 3. In general, every arc on a given specimen exhibited a different pattern compared to all other arcs, although some parts of an arc might repeat, especially near an edge. In addition, when punchthrough holes occurred, they repeatedly formed bright focal points for the discharges.

The Kapton damage photographs were all taken on a single specimen 75 μm thick which had been subjected to 11 discharges. Figure 4 shows a groove disappearing into a heaved-surface tunnel, indicating that groove and tunnel damage both result from the some basic physical process. Figure 5 includes the area of Figure 4 in its lower right quadrant and shows that the heaved-surface tunnel comprises a narrow central channel bordered by a damaged fringe. Figures 6 and 7 show surface grooves crossing heaved-surface tunnels, while Figures 8 and 9 for the same region show additional tunnels with no surface heaving.

The Teflon specimen examined was 50 μm thick and had been subjected to 9 discharges, but nevertheless damage was difficult to find except at a punchthrough and near an edge. The latter damage is shown in Figure 10 in which discharge tunnel heaving and cracking is clearly evident.

The Mylar specimen tested was 75 μm thick and had been subjected to 12 discharges, resulting in damage which was relatively easy to find. Figures 11 and 12, taken near the mask edge, show a variety of surface patterns which are displayed at higher magnification in Figures 13 and 14. Figure 15 is a good example of a branched groove crossing a heaved-surface tunnel, while Figure 16 shows both straight grooves and a leafy pattern of irregular grooves. Finally, Figures 17, 18 and 19 provide close-up views of blowout holes in a heaved-surface tunnel, the appearance of the holes suggesting localized melting of the Mylar.

4. CONCLUSIONS

Damage photographs on Kapton, Teflon and Mylar consistently reveal channel-like patterns. The subsurface channels (or tunnels) are always irregular and often result in surface heaving and cracking with occasional blowout holes. The surface channels are usually grooves in a pattern of straight branching lines suggesting surface crystallization effects, but sometimes an irregular leafy pattern of surface grooves can be seen interspersed amongst the straight grooves. Surface grooving on Teflon can sometimes be seen in microscopic examination but the grooves are too faint to photograph well.

Damage in the form of channels suggests the ejection of ionized discharge debris along these channels, especially in the case of tunnels. It is postulated that the rate of excess charge removal along the plasma channel determines the rate at which the discharge is permitted to progress, and that the transport of charge along the channel involves an approximately dispersionless wave propagation mode which is much slower than the velocity of light. It is shown that this mode can propagate in the case of an overdense plasma, and that the presence of a nearby ground plane does not strongly influence the properties of the mode.

5. ACKNOWLEDGMENTS

The author expresses his gratitude to G.R. Dubois for his contributions to the experiments and the photography. The research was supported by the Natural Sciences and Engineering Research Council of Canada under Grant A-4140.

6. REFERENCES

1. Rosen, A. (Ed.), Spacecraft Charging by Magnetospheric Plasmas, Progress in Astronautics and Aeronautics, Vol. 47, 1976.

2. Pike, C.P., and Lovell, R.R. (Eds.), Proceedings of the 1976 Spacecraft Charging Technology Conference, Report AFGL-TR-77-0051/NASA TMX-73537, 24 Feb. 1977.

3. Goodman, J.M. (Ed.), Effect of the Ionosphere on Space and Terrestrial Systems, Proceedings of an NRL/ONR-sponsored conference held in Arlington, Va., January 24-26, 1978. U.S. Gov't. Printing Office Stock No. 008-051-00069-1.

4. Spacecraft Charging Technology - 1978, Proceedings of a conference held at Colorado Springs, Oct. 31 to Nov. 2, 1978, edited by R.C. Finke and C.P. Pike, NASA Conference Publication 2071/AFGL-TR-79-0082.

5. Balmain, K.G., Kremer, P.C., and Cuchanski, M., "Charged-Area Effects on Spacecraft Dielectric Arc Discharges", in Reference 3, pp. 302-308.

6. Balmain, K.G., "Scaling Laws and Edge Effects for Polymer Surface Discharges", in Reference 4, pp. 646-656.

7. Yadlowsky, E.J., Hazelton, R.C., and Churchill, R.J., "Characterization of Electrical Discharges on Teflon Dielectrics Used as Spacecraft Thermal Control Surfaces", in Reference 4, pp. 632-645.

8. Balmain, K.G., and Dubois, G.R., "Surface Discharges on Teflon, Mylar and Kapton", paper G-10 presented at the 1979 IEEE Nuclear and Space Radiation Effects Conference, Santa Cruz, California, July 17-20, 1979.

9. Amore, L.J., and Eagles, A.E., "Materials and Techniques for Spacecraft Static Charge Control", in Reference 2, 621-654.

10. Inouye, G.T., and Sellen, J.M., "A Proposed Mechansim for the Initiation and Propagation of Dielectric Surface Discharges", in Reference 3, pp. 309-312.

11. Leadon, R., and Wilkenfeld, J., "Model for Breakdown Process in Dielectric Discharges", in Reference 4, pp. 704-710.

12. Budenstein, P.P., "Dielectric Breakdown in Solids", Report AD-A012 177, prepared for the U.S. Army Missile Command, Redstone Arsenal, Alabama, 20 December 1974.

13. Meulenberg, A., "Evidence for a New Discharge Mechanism for Dielectrics in a Plasma", in Reference 1, pp. 237-246.

14. Beers, B.L., Hwang, H.-C., Lin, D.L., and Pine, V.W., "Electron Transport Model of Dielectric Charging", in Reference 4, pp. 209-238.

15. Johnson, C.C., Field and Wave Electrodynamics, McGraw-Hill Book Co., N.Y., 1965, pp. 173-176.

16. Beers, B.L., Pine, V.W., Hwang, H.C., and Bloomberg, H.W., "Negative Streamer Development in FEP Teflon", Paper G-7 presented at the 1979 IEEE Nuclear and Space Radiation Effects Conference, Santa Cruz, California, July 17-20, 1979.

17. Flanagan, T.M., Denson, R., Mallon, C.E., and Treadaway, M.J., "Effect of Laboratory Simulation Parameters on Spacecraft Dielectric Discharges", paper G-8 presented at the 1979 IEEE Nuclear and Space Radiation Effects Conference, Santa Cruz, California, July 17-20, 1979.

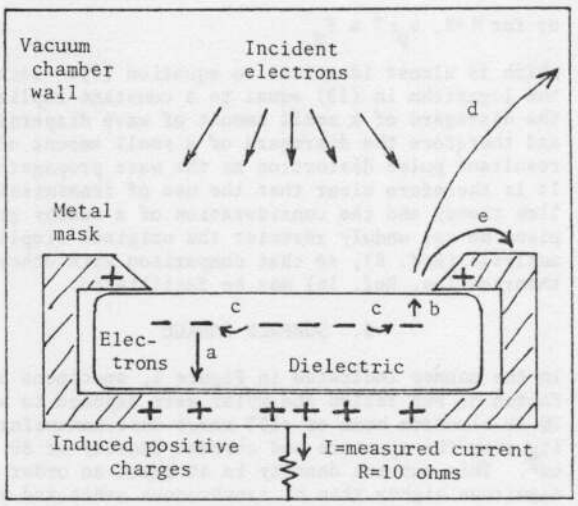

Figure 1. Possible charging and discharging phenomena: a) punchthrough arc with top surface of dielectric blown off, b) blowoff arc to surface, c) flashover arc or propagating subsurface discharge, d) ejected electrons going to chamber wall, e) ejected electrons going to mask.

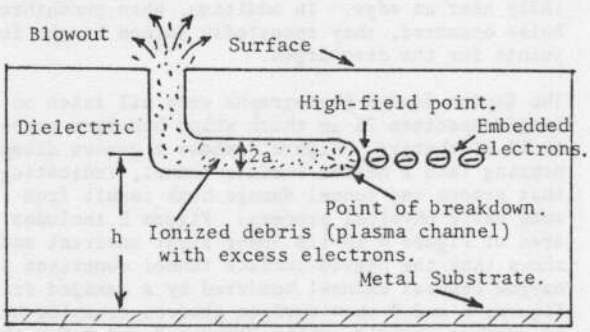

Figure 2. The propagation of a breakdown channel through a subsurface layer of electrons embedded in a dielectric sheet.

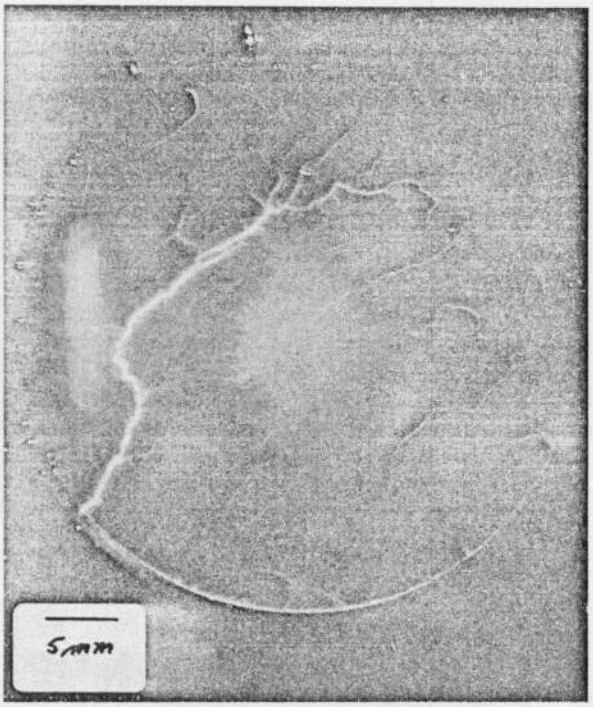

Figure 3. Typical arc discharge on Mylar.

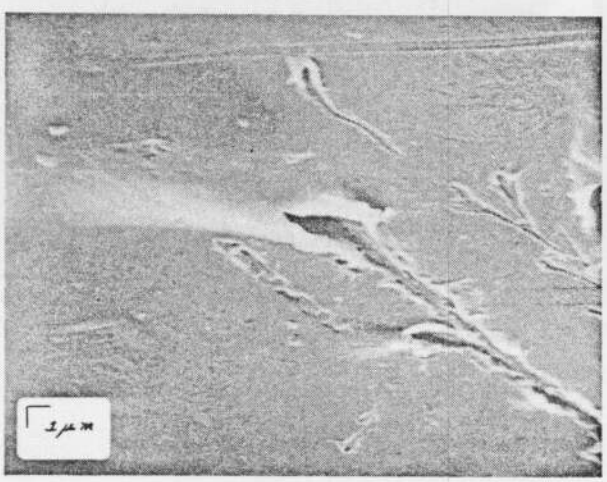

Figure 4. Kapton; scanning electron microscope.

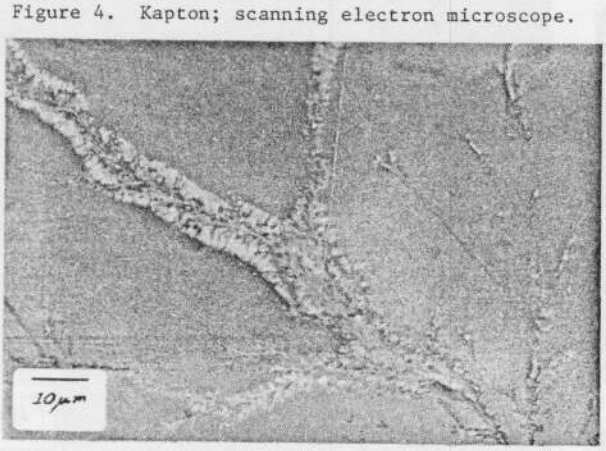

Figure 5. Kapton; reflected light.

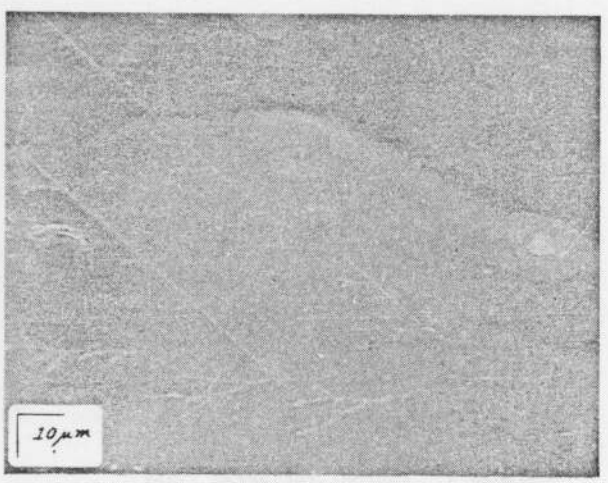

Figure 6. Kapton; scanning electron microscope.

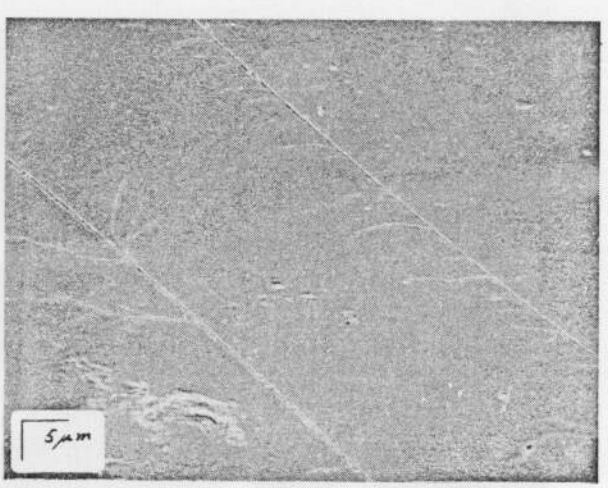

Figure 7. Kapton; scanning electron microscope.

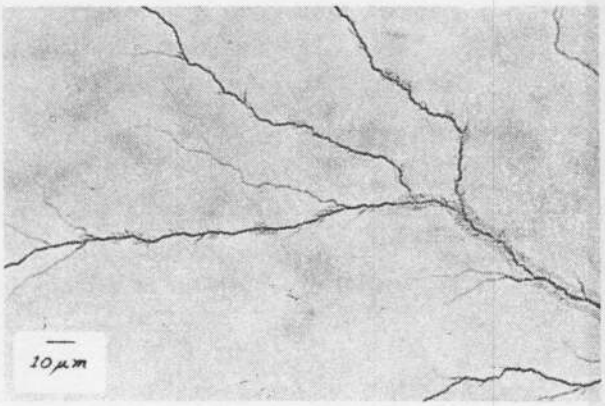

Figure 8. Kapton; transmitted light.

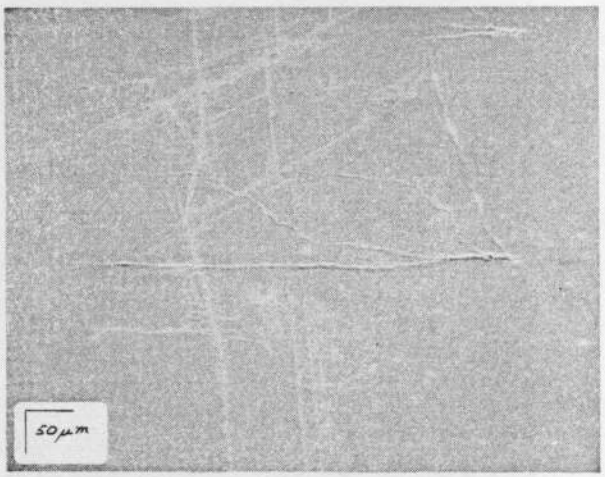

Figure 11. Mylar; scanning electron microscope.

Figure 9. Kapton; reflected light.

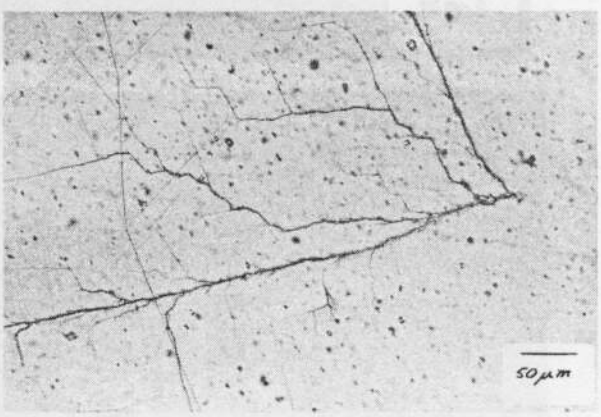

Figure 12. Mylar; transmitted light.

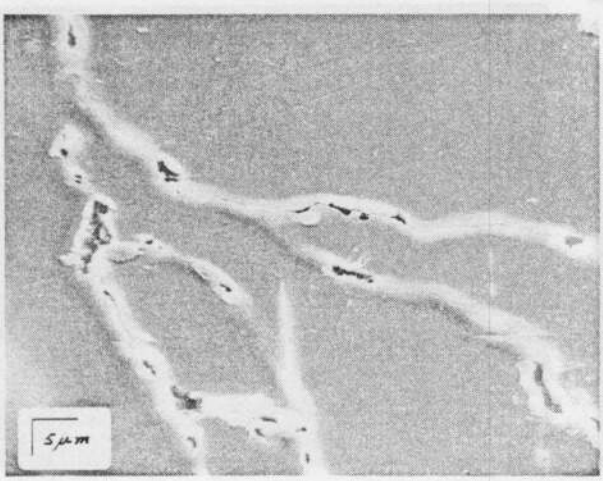

Figure 10. Teflon; scanning electron microscope.

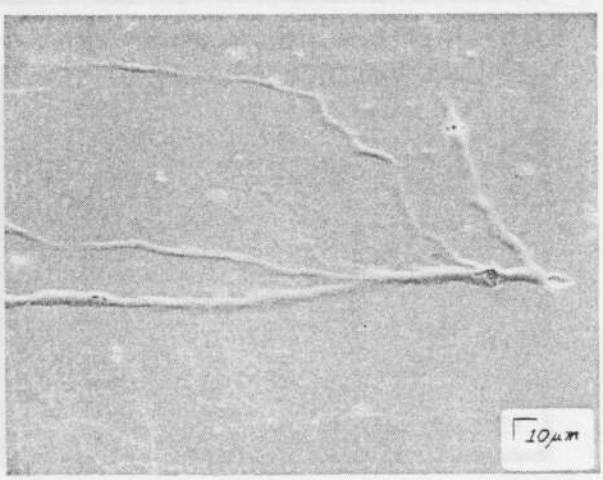

Figure 13. Mylar; scanning electron microscope.

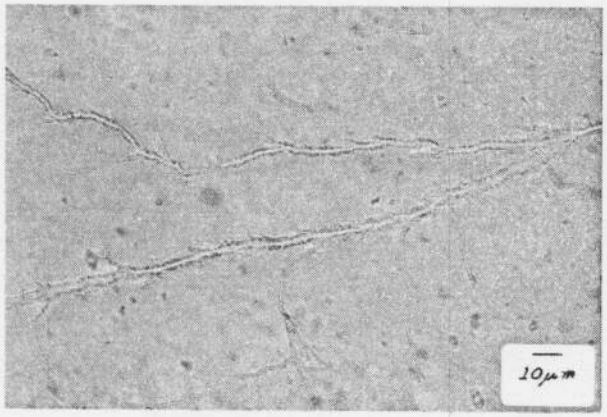

Figure 14. Mylar; reflected light.

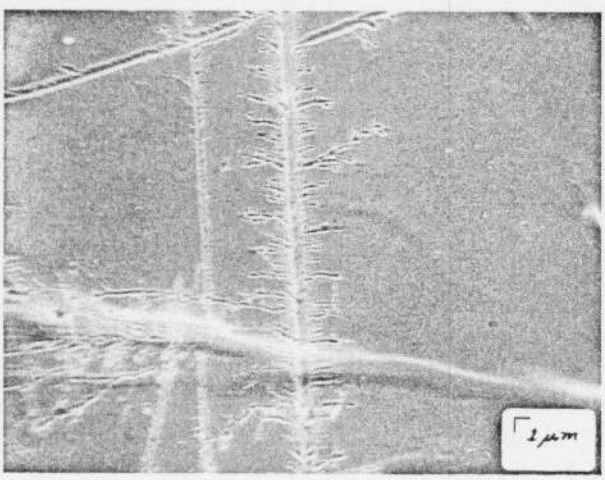

Figure 15. Mylar; scanning electron microscope.

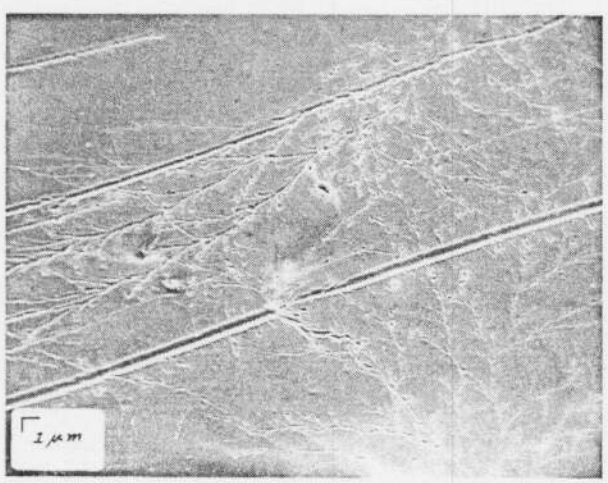

Figure 16. Mylar; scanning electron microscope.

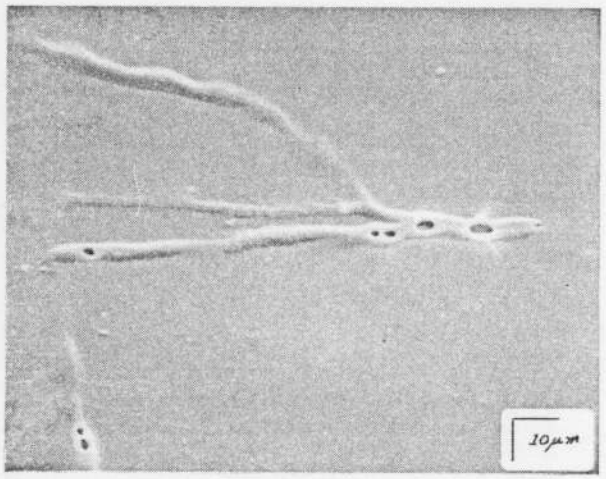

Figure 17. Mylar; scanning electron microscope.

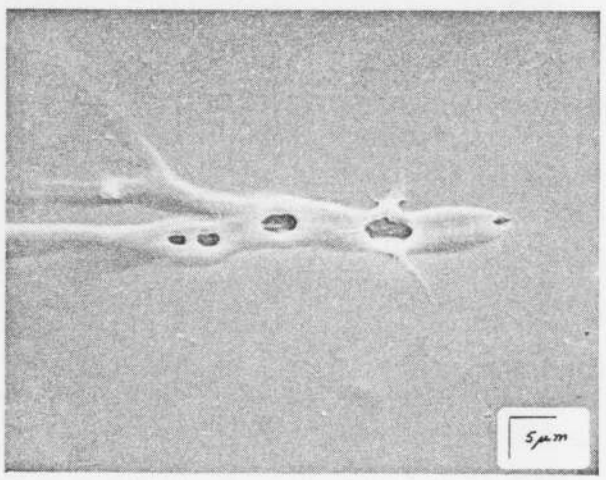

Figure 18. Mylar; scanning electron microscope.

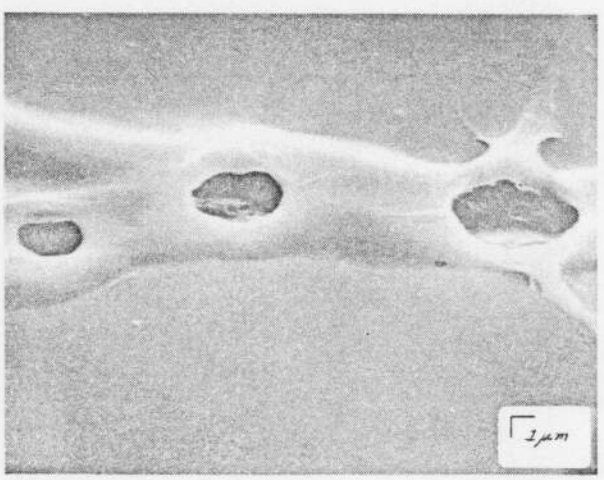

Figure 19. Mylar; scanning electron microscope.